

Article

Analysis of Flow Characteristics of a Debris Filter in a Condenser Tube Cleaning System

Da-Woon Jung ¹, Chung-Won Seo ¹, Young-Chan Lim ¹, Dong-Sun Kim ², Seung-Yul Lee ² and Hyun-Kyu Suh ^{3,*}

¹ Graduate School of Mechanical Engineering, College of Engineering, Kongju National University, 1223-23 Cheonan-daero, Cheonan-si 31080, Republic of Korea; dwjung@smail.kongju.ac.kr (D.-W.J.); cwseo@smail.kongju.ac.kr (C.-W.S.); yclim@ync.ac.kr (Y.-C.L.)

² Jeong-Woo Industrial Machine Co., Ltd., 253,5 Sandan-ro, Susin-myeon, Dongnam-gu, Cheonan-si 31251, Republic of Korea; dskim@jimc.co.kr (D.-S.K.); leesy@jimc.co.kr (S.-Y.L.)

³ Division of Mechanical & Automotive Engineering, Kongju National University, 1223-24 Cheonan-daero, Cheonan-si 31080, Republic of Korea

* Correspondence: hksuh@kongju.ac.kr; Tel.: +82-41-521-9264

Abstract: In a power plant that uses seawater as a coolant, a debris filter (DF) is required to remove foreign substances from the seawater, and differential pressure leads to a decrease in the coolant flow rate, leading to a decrease in the power generation efficiency. In this study, an analysis was performed for the cases wherein the initial flow velocity conditions of the DF used in the condenser tube cleaning system (CTCS) were 1.5 m/s, 2.0 m/s, and 2.5 m/s using Ansys Fluent 2021, and the flow characteristics were identified. The flow and differential pressure characteristics of a CTCS with an installed DF were considered in a comparative analysis of the velocity, pressure, and turbulence kinetic energy (TKE) distributions. The results confirmed that a vortex was generated in the pipe with the DF, apparently due to the collision of the flow with the bracket of the DF. As the flow rate increased, the range of the vortex increased, causing a loss in flow.

Keywords: condenser tube cleaning system (CTCS); debris filter (DF); differential pressure; fluid resistance; pressure drop; turbulence kinetic energy (TKE); flow vortex



Citation: Jung, D.-W.; Seo, C.-W.; Lim, Y.-C.; Kim, D.-S.; Lee, S.-Y.; Suh, H.-K. Analysis of Flow Characteristics of a Debris Filter in a Condenser Tube Cleaning System. *Energies* **2023**, *16*, 4472. <https://doi.org/10.3390/en16114472>

Academic Editor: Rob J.M. Bastiaans

Received: 9 April 2023

Revised: 5 May 2023

Accepted: 24 May 2023

Published: 1 June 2023



Copyright: © 2023 by the authors. Licensee MDPI, Basel, Switzerland. This article is an open access article distributed under the terms and conditions of the Creative Commons Attribution (CC BY) license (<https://creativecommons.org/licenses/by/4.0/>).

1. Introduction

Due to the indiscriminate use of primary energy sources such as oil, coal, natural gas, and nuclear power caused by advanced industrialization, the depletion of fossil fuels is imminent, and there is no alternative to meet the current energy demand for fossil fuels. Moreover, due to environmental problems caused by global warming, the productivity and technological importance of the energy industry are becoming increasingly important. In particular, for countries that need to import resources and convert them into secondary energy to produce electricity, efficient development based on economic stability is essential [1–4]. Janis et al. conducted research on reducing greenhouse gas emissions and efficient energy systems. They confirmed that reducing greenhouse gas emissions provides a large amount of electricity and that SMRs can be combined with renewable energy sources to create a hybrid energy system, thus increasing efficiency [5]. Ivan et al. conducted a comparative analysis study on the ACNA 600-35 pumping device developed for improving the energy efficiency of nuclear power plants compared to similar products. They compared the results of the pressure distribution and relative velocity and confirmed that the energy efficiency was improved compared to the comparison product [6].

One of the most influential pieces of equipment in power plants, the condenser plays a role in increasing efficiency by rotating the turbine and generator with high-pressure and high-temperature steam and is very important for energy production because it reuses steam.

In the literature, studies have been conducted to improve the performance of capacitors by utilizing various parameters. Ibrahim et al. studied the effect of the fouling of condenser tubes on the thermal performance in nuclear power plants and found that an increase in the fouling factor causes a decrease in thermal efficiency and power loss [7]. Alabrudzinski et al. performed simulations based on computational fluid dynamics (CFD) analysis using the fouling thermal resistance value according to the fouling growth rate measurement results and turbine operating conditions. They found that the thermal resistance of fouling reduces the output of the turbine and that even an old condenser can affect the output of the turbine [8]. Pattanayak et al. analyzed various parameters that affect the efficiency of steam condensers through simulation models based on thermodynamic theory. They derived the cooling water temperature that can maintain the optimal condenser pressure and found that as the cooling water temperature increases, the heat rate of the power cycle decreases [9]. Mohammadaliha et al. developed a new air-to-liquid crossflow heat exchanger model to analyze the effect of thermal conductivity on the overall efficiency in condenser heat exchangers. They found that materials with excellent corrosion resistance and low-cost materials have low thermal characteristics that affect the performance and that if materials with a thermal conductivity value of less than $0.5 \text{ W/m}\cdot\text{K}$ are used, the efficiency of heat recovery systems is significantly reduced [10]. Gadhamshetty et al. used a new approach, a cooling water heat energy storage system, to improve the performance degradation due to an ambient temperature rise, which is a disadvantage of air-cooled condensers (ACC) environmentally compared to water-cooled condensers in heat dissipation. They confirmed that power loss can be reduced through thermodynamic modeling and simulation [11].

Most power plants use seawater as a coolant, which introduces various impurities and foreign substances such as seaweed and fish eggs into the seawater. This provides an environment for microbial growth, and the impurities adhere to the surface of the condenser tube, reducing the heat exchange performance of the condenser and increasing the exhaust pressure of the steam turbine, which can cause safety issues and lead to a decrease in power generation efficiency and power production efficiency [12]. To solve this, as shown in Figure 1, the DF is installed in front of the condenser to filter the seawater. The DF is composed of a screen, rotor, and hopper. It filters foreign substances contained in seawater using a screen and absorbs and removes the various foreign substances that accumulate using a rotor and hopper. However, in this process, foreign substances that are filtered by the screen and accumulate can create a differential pressure. This can decrease the flow rate of cooling water flowing into the condenser, which leads to a decrease in the heat exchange efficiency of the condenser and the stability of the circulating water pump [13,14].

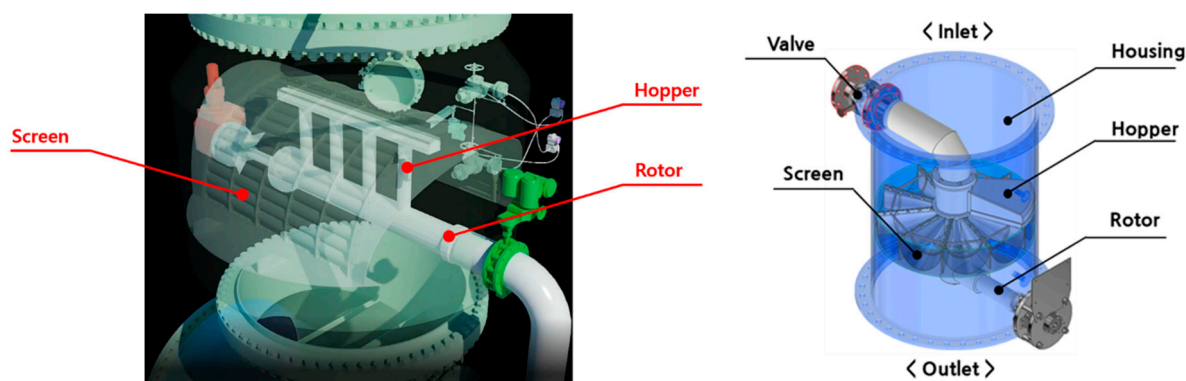


Figure 1. The shape and position of the DF inside the CTCS.

Until recently, research to improve the condenser heat exchange performance has primarily focused on improving the recovery and circulation rate of sponge balls and reducing ball loss by considering the flow characteristics of the CTCS in which the sponge balls are applied [12,15,16]. Jung et al. conducted the DF flow tests for two types of DF,

P-grid and G-grid, using 18 types of debris. They found that the G-grid filter design showed better performance than the P-grid design because it provided a smaller flow area and higher grid strap than the P-grid design [17]. In addition, Walker et al. analyzed the economic impact of fouling on the condenser to analyze the cleaning system for economic cost analysis and found that increasing the cleaning frequency can reduce additional fuel costs due to fouling [18]. In another work, Chae et al. conducted an experimental study to maintain the efficiency of plate heat exchangers while eliminating the inconvenience of cleaning operations and measured the recovery rate according to changes in the flow rate within the tube and changes in the cleaning time and recovery time [1]. Kim et al. conducted an experiment-based study to solve the stability problem caused by excessive vibration during circulating water pump operation. They revealed how the operating characteristics of the DF affected the natural vibration of the pump and suggested ways to reduce vibration [19].

In this study, research was conducted to improve the performance of the CTCS equipped with a DF that is currently installed in existing power plants. Due to the pressure drop caused by fluid pressure, which limits the stability of the fluid pump and the efficiency of heat exchange, numerical analysis was performed to analyze the flow characteristics inside the system's pipes and identify factors affecting the pressure and fluid resistance. It was confirmed that the pressure drop caused by the screen that filters out the DF and external substances is a factor that affects it, and by analyzing the correlation between the shape of the screen that can minimize the pressure drop and the size of the perforated plate, we derived an optimal screen shape according to the DF size through CFD analysis. In addition, the effects of the presence or absence of the filter on flow characteristics and differential pressure performance in the pipe according to each initial flow rate condition were compared and analyzed, and the velocity, pressure, and TKE distribution in the pipe according to the flow rate were examined for comparison and analysis.

2. Numerical Analysis Method

2.1. Numerical Analysis Target and Design Conditions

This study was conducted to investigate the effect of the presence or absence of the DF and the flow velocity on the differential pressure and TKE. Numerical analysis modeling was performed using a 14-inch DF that was actually in use, as shown in Figure 2a. The height of the mid-plate and the size of the perforated plate for fixing the screen were set to 30 mm, as shown in Figure 2b. Fluid analysis was conducted using commercial code and the fluid region of Figure 2a was extracted to create a mesh for analysis. The fluid properties used in the analysis were based on H₂O. In addition, as shown in Figure 2c, to derive the results of the velocity, pressure, and TKE, the vertical direction (H) was set at an interval of 0.06 m, and the horizontal direction (L) was set at 0.333 m intervals from the bottom of the inlet in the center plane of the pipe. Each of the points used for measuring flow characteristics is plotted in this figure, and the conditions were set with the goal of establishing a numerical analytical database for the shape.

2.2. Governing Equations for Numerical Analysis

The governing equations for flow analysis, continuity equations, momentum equations, and energy equations were applied, and they are expressed as the following equations:

$$\frac{\partial u}{\partial x} + \frac{\partial v}{\partial y} + \frac{\partial w}{\partial z} = 0 \quad (1)$$

$$\begin{aligned} u \frac{\partial u}{\partial x} + v \frac{\partial v}{\partial y} + w \frac{\partial w}{\partial z} &= -\frac{\partial p}{\partial x} \frac{1}{\rho} + \nu_e \left(\frac{\partial^2 u}{\partial x^2} + \frac{\partial^2 u}{\partial y^2} + \frac{\partial^2 u}{\partial z^2} \right) \\ u \frac{\partial u}{\partial x} + v \frac{\partial v}{\partial y} + w \frac{\partial w}{\partial z} &= -\frac{\partial p}{\partial x} \frac{1}{\rho} + \nu_e \left(\frac{\partial^2 v}{\partial x^2} + \frac{\partial^2 v}{\partial y^2} + \frac{\partial^2 v}{\partial z^2} \right) \\ u \frac{\partial u}{\partial x} + v \frac{\partial v}{\partial y} + w \frac{\partial w}{\partial z} &= -\frac{\partial p}{\partial x} \frac{1}{\rho} + \nu_e \left(\frac{\partial^2 w}{\partial x^2} + \frac{\partial^2 w}{\partial y^2} + \frac{\partial^2 w}{\partial z^2} \right) \end{aligned} \quad (2)$$

$$u \frac{\partial T}{\partial x} + v \frac{\partial T}{\partial y} + w \frac{\partial T}{\partial z} = \alpha \left(\frac{\partial^2 T}{\partial x^2} + \frac{\partial^2 T}{\partial y^2} + \frac{\partial^2 T}{\partial z^2} \right) \quad (3)$$

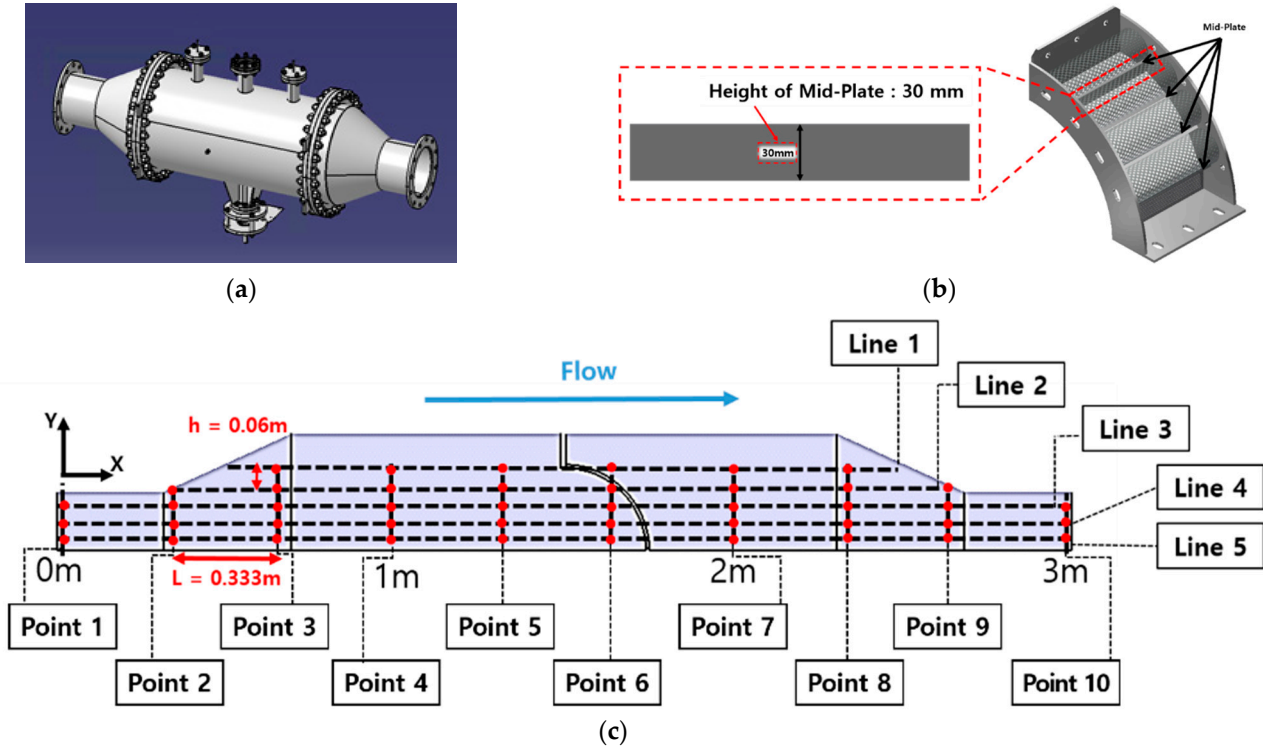


Figure 2. Schematics of the DF and flow characteristics measuring points: (a) schematics of the DF; (b) shape and size of the plate; (c) measuring points of pipe with the DF applied.

In Equations (1) to (3), u , v , and w represent the speed in the x , y , and z directions, respectively, ρ is the density, and ν is the coefficient of kinematic viscosity. For the turbulence model, the shear-stress transport (SST) model suitable for the $k - \omega$ model-based flow separation simulation is applied, and the flow field is calculated based on the TKE (k) and energy-specific dissipation rate (ω) equations.

$$\frac{\partial}{\partial t}(\rho k) + \frac{\partial}{\partial x_i}(\rho k u_i) = \frac{\partial}{\partial x_j} \left[\Gamma_k \frac{\partial k}{\partial x_j} \right] + G_k + G_b - Y_k + S_k \quad (4)$$

$$\frac{\partial}{\partial t}(\rho \omega) + \frac{\partial}{\partial x_i}(\rho \omega u_i) = \frac{\partial}{\partial x_j} \left[\Gamma_\omega \frac{\partial \omega}{\partial x_j} \right] + G_\omega + G_{\omega b} - Y_\omega + S_\omega \quad (5)$$

G_k represents the generation of the TKE due to the velocity gradient, and G_ω is the energy-specific dissipation rate (ω) generation term. Γ_k and Γ_ω mean the effective diffusion of k and ω due to turbulence, Y_k and Y_ω are the dissipation terms of k and ω due to turbulence, S_k and S_ω are user-defined terms, and the Eddy viscosity in the $k - \omega$ turbulence model $\mu_t = \rho k / \omega$ is calculated. The SST $k - \omega$ model activates the $k - \omega$ model near the wall and activates the $k - \epsilon$ model away from the wall to produce results. This technique of using two models is called blending and is more accurate than other turbulence models and effective in interpreting flow near walls, so it was applied in this study [20,21].

2.3. Verification of Numerical Analysis Results

Before numerical analysis, about 1.3 million tetra meshes were generated by extracting the fluid area in the pipe to which a 14-inch DF was applied. Detailed information about the mesh applied to the numerical analysis is shown in Table 1 and Figure 3. Based on the differential pressure results for each flow velocity obtained in the experiment, the differential pressure displayed by the screen (perforated plate) in the DF was simulated to be the viscous resistance value of a porous zone, similar to the experimental value. The normalized differential pressure results are shown in Figure 4. After normalization, it was confirmed that the errors at the initial flow rates of 1.5 m/s, 2 m/s, and 2.5 m/s were 0%, 1.09%, and 6.99%, respectively. Additionally, the trend in the experimental values and numerical analysis was consistent across all flow rate conditions. Therefore, the reliability and importance of this study have been secured.

Table 1. The amount of mesh used for the numerical analysis.

Cases	Nodes	Elements
With DF	260,950	1,308,948
Without DF	51,297	259,098

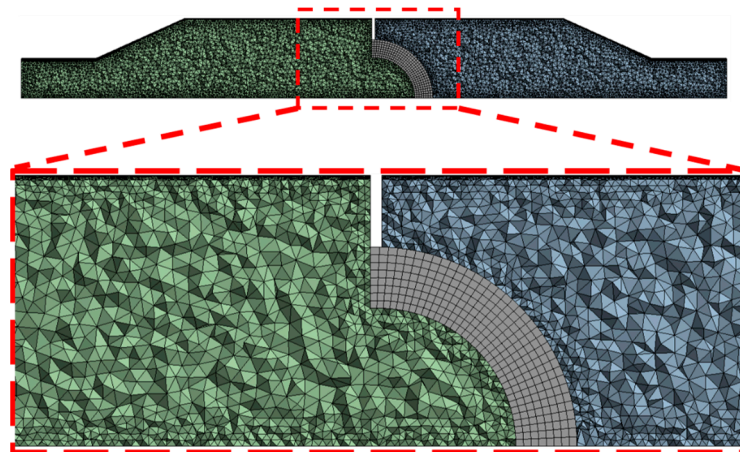


Figure 3. Mesh of pipe with the DF applied.

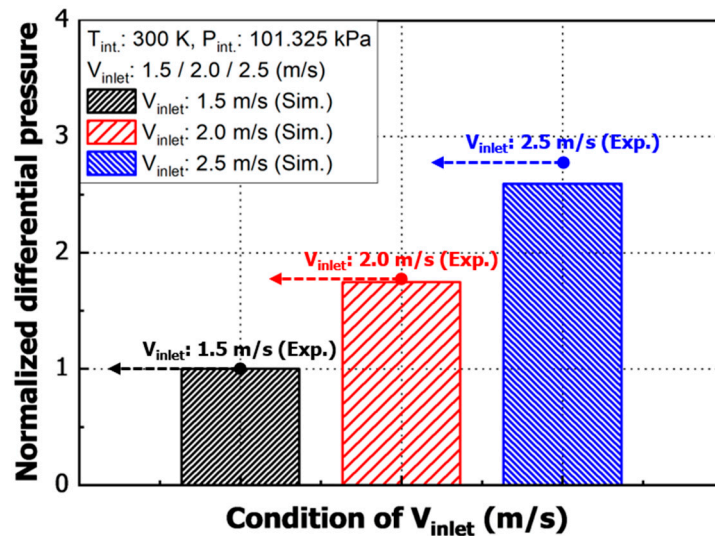


Figure 4. Normalized results for differential pressure under various flow velocities.

2.4. Experimental Method and Conditions

This experiment was conducted to verify the performance of CTCS affected by DF, and the experimental device was configured as shown in Figure 5a. To perform the differential pressure performance test, a main pump that controls the flow rate according to the initial flow rate condition and a gear motor and motor inverter for rotating the rotor and hopper of the existing DF design product were configured. As can be seen in Table 2, the flow rate conditions applied in the experiment were 1.5 m/s, 2 m/s, and 2.5 m/s, which are the same as the numerical analysis conditions, and the actual experimental device was as shown in Figure 5b.

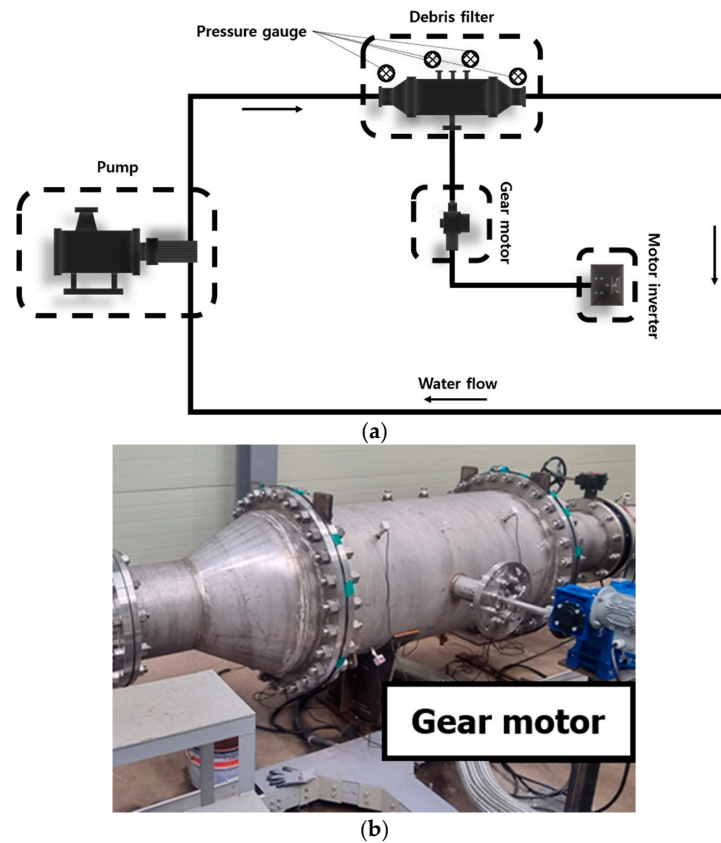


Figure 5. Experimental apparatus for debris filter test. (a) Schematic of DF experiment; (b) experimental gear motor for DF.

Table 2. The differential pressure experiment results for each flow velocity.

Velocity (m/s)	Differential Pressure (kPa)
1.5	6.05
2	10.78
2.5	16.87

2.5. Numerical Analysis Conditions

Steady-state analysis was carried out by applying the analysis conditions shown in Table 3, based on the grid used to verify the analysis results. To analyze the TKE and differential pressure characteristics in the presence or absence of the DF, a numerical analysis was performed on the pipe of the CTCS with or without 14-inch DF cases. The working fluid was set as water, and the flow rates were 1.5 m/s, 2.0 m/s, and 2.5 m/s. Then, the flow characteristics in the CTCS were compared and analyzed according to the flow rates.

Table 3. Numerical analysis conditions.

Contents	Conditions
Turbulence model	$k - \omega$ (sst)
Inlet velocity (m/s)	1.5, 2.0, 2.5
Inlet temperature (K)	300
Inlet pressure (kPa)	101.325
Outlet condition	Pressure outlet

3. Numerical Analysis Results

3.1. Effect of the DF on Flow Rate

Figure 6 shows the velocity distributions in the pipe with and without the DF applied, and Figure 7 shows the velocity values in the pipe according to the inlet flow rate change as velocity vectors. In the velocity distribution when the DF was on the left side of Figure 6, the main flow at the front end before passing the filter was distributed in the center of the pipe. Without the DF on the right side of Figure 6, the main flow was distributed near the wall of the pipe. The streamline in Figure 6 indicates that the main flow forms in the center of the tube because a vortex is generated by the flow colliding with the bracket at the top of the DF.

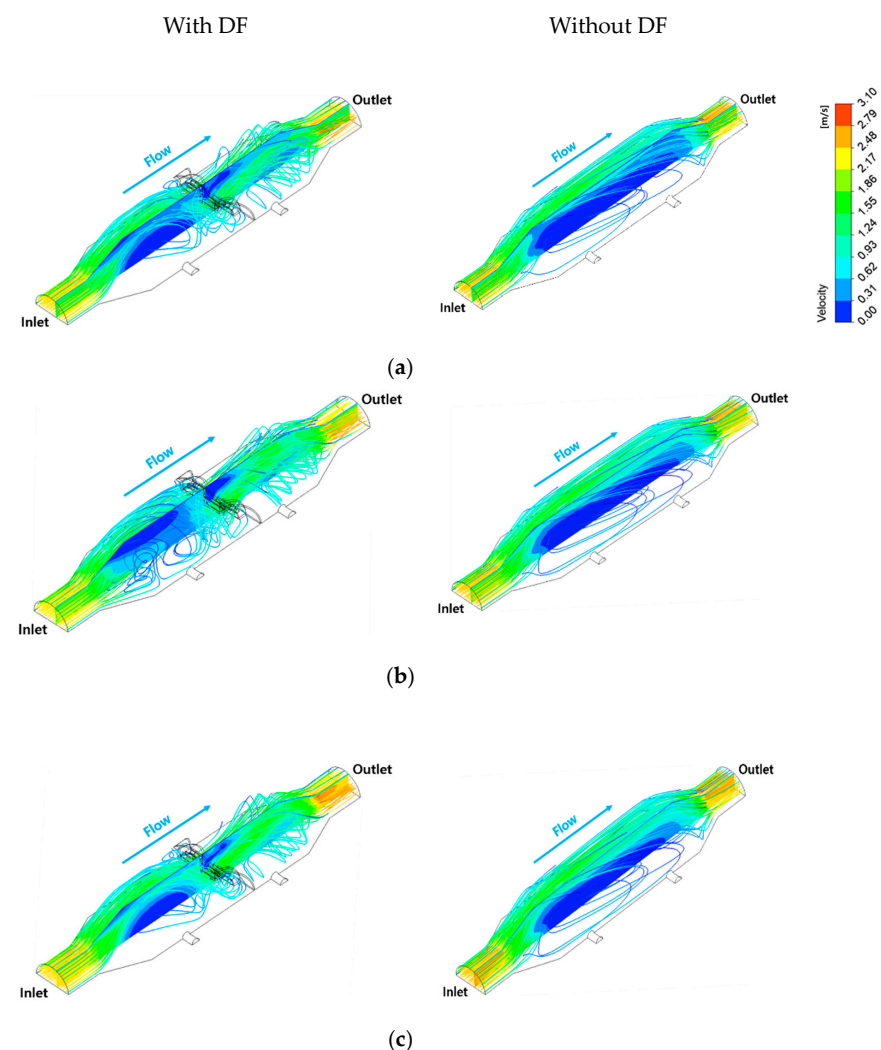


Figure 6. Comparison results of velocity contour with the DF (left) and without the DF (right). (a) $V_{\text{inlet}} = 1.5$ m/s; (b) $V_{\text{inlet}} = 2.0$ m/s; (c) $V_{\text{inlet}} = 2.5$ m/s.

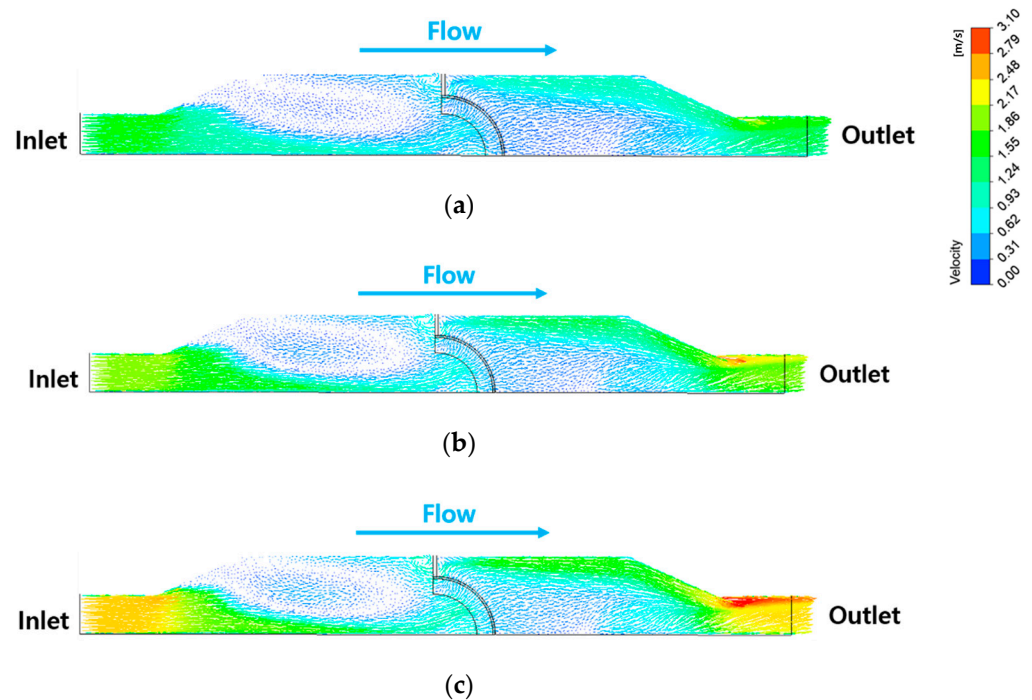
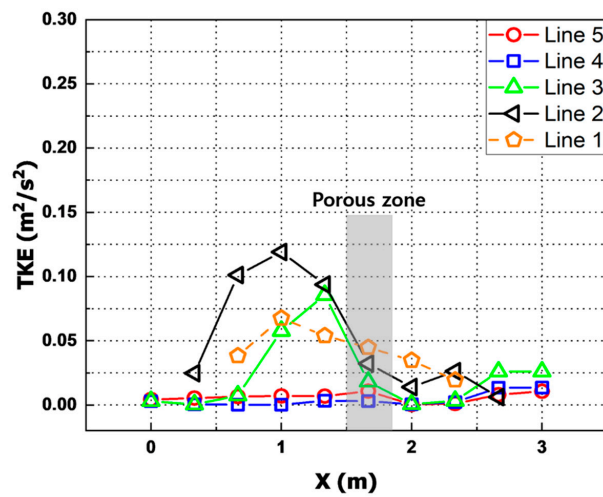


Figure 7. The velocity vector in a pipe with the DF. (a) $V_{\text{inlet}} = 1.5$ m/s; (b) $V_{\text{inlet}} = 2.0$ m/s; (c) $V_{\text{inlet}} = 2.5$ m/s.

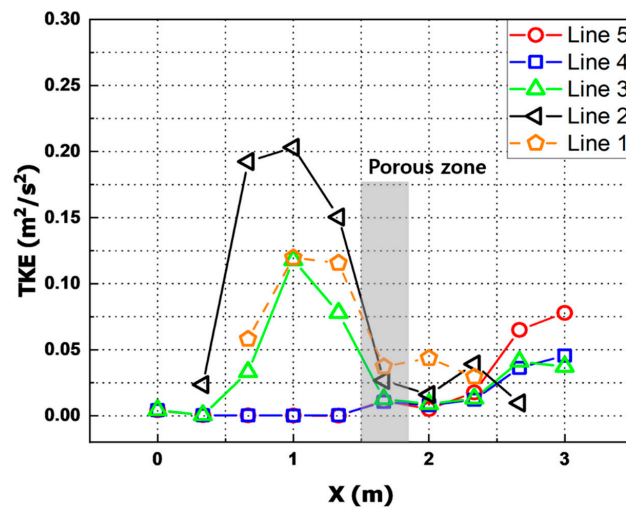
Figures 8 and 9 show the distribution of TKE and velocity in the tube of the CTCS with the DF. As shown in Figure 8, the TKE rapidly increases at the front end of the filter set as the porous zone. This suggests that the main flow increases the resistance of the working fluid due to the viscous resistance of the porous zone. As the vortex generated by the flow colliding with the bracket at the top of the filter grows, it increasingly interferes with the main flow.

Additionally, in the 2.5 m section in Figure 8, the TKE in Lines 3, 4, and 5 shows a tendency to increase again. This is because, as shown in the velocity distribution in the 2 m-to-2.5 m section in Figure 9, the velocity of the main flow distributed along the wall of the tube increases due to the shape of the nozzle-shaped tube. The TKE increases as it affects the main flow due to the interaction with the relatively slower flow distributed in the center of the tube. The analyses confirmed that when the DF is applied, the main flow at the rear end is distributed along the wall of the tube, in contrast to the front end. This is because the bracket located on the top of the filter acts as a barrier, and the pressure at the rear end of the bracket is relatively lower than the pressure immediately after the porous zone. The working fluid that has passed through the filter tends to accelerate to the top of the filter with low pressure. This is judged to be the same as the tendency that the flow velocity of Line 1, the outer tube of the pipe at the point 2 m past the porous zone, appears to be higher than other points under all flow velocity conditions in Figure Line 3 in Figure 8c under the 2.5 m/s flow rate, unlike (a) and (b), is similar to the trend in Lines 4 and 5 at the front of the porous zone. This indicates that as the flow rate increases, the range of the main flow increases, so the trend in Line 3 became similar to the flow at the center of the pipe.

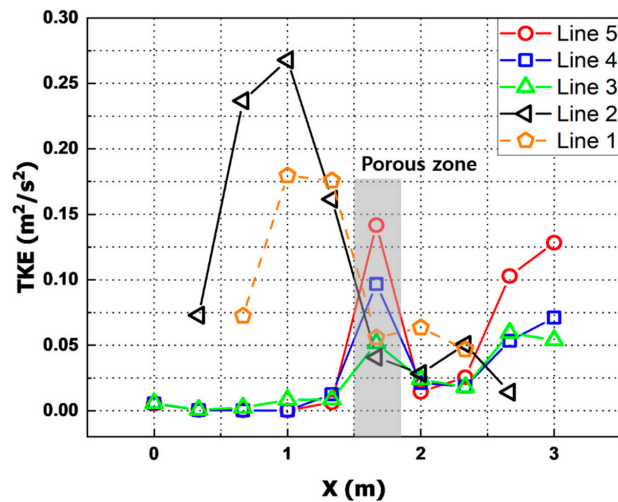
Figure 10 shows the distributions of TKE concerning the flow velocity in the pipe with the DF applied. As the flow velocity increases, the effect of the area and value of the TKE at the front of the filter on the main flow increases, and it can be inferred that the distributions of the vortex increase. As the flow velocity increases, the radius of the vortex resulting from the flow colliding with the bracket at the top of the filter increases, and the friction with the main flow increases, showing the trend in Figure 10c.



(a)

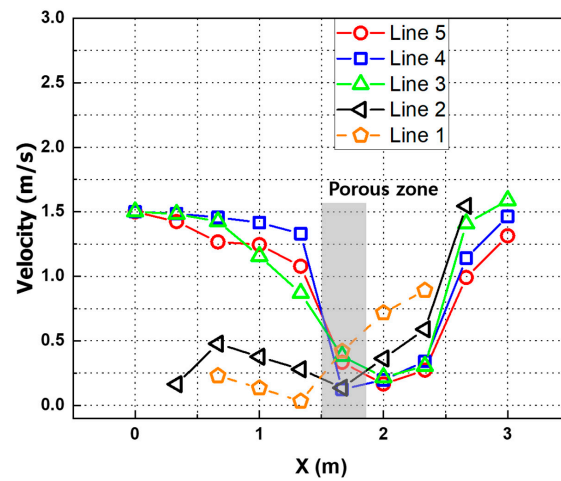


(b)

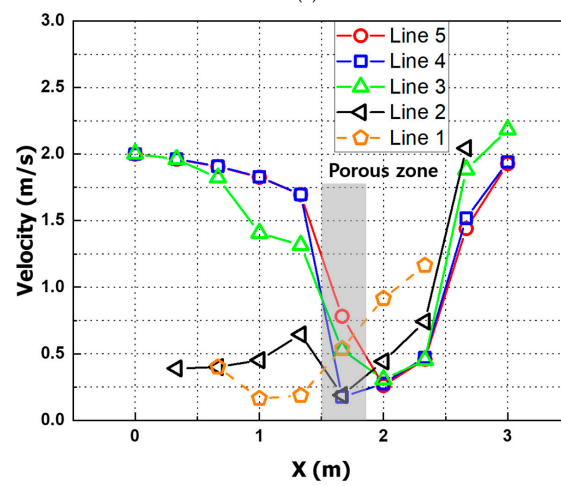


(c)

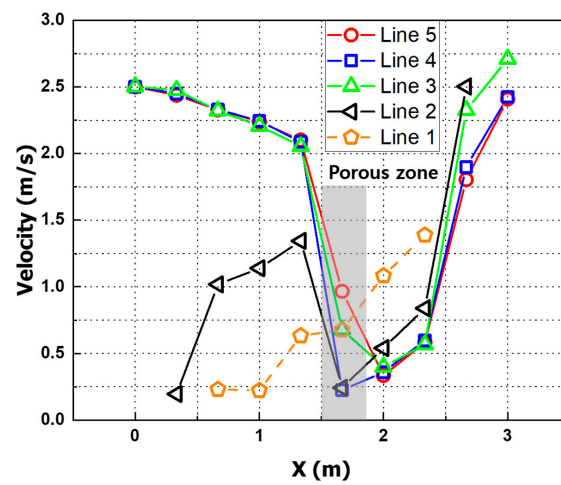
Figure 8. The TKE distributions of pipe with DF applied. (a) $V_{inlet} = 1.5 \text{ m/s}$; (b) $V_{inlet} = 2.0 \text{ m/s}$; (c) $V_{inlet} = 2.5 \text{ m/s}$.



(a)



(b)



(c)

Figure 9. The velocity distributions of pipe with the DF applied. (a) $V_{inlet} = 1.5$ m/s; (b) $V_{inlet} = 2.0$ m/s; (c) $V_{inlet} = 2.5$ m/s.

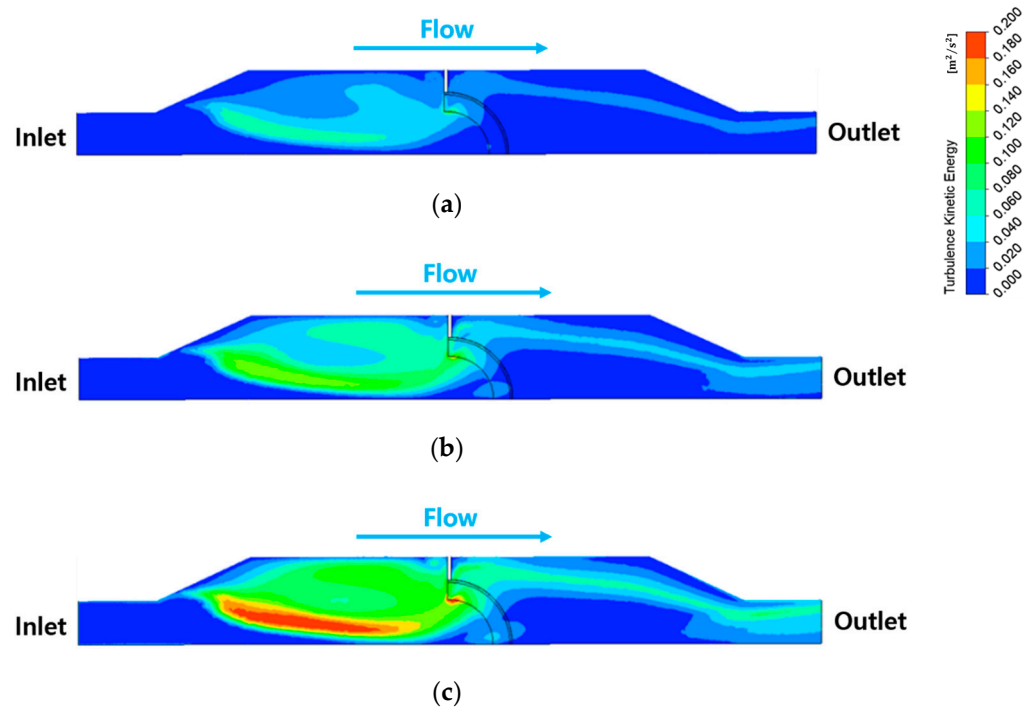


Figure 10. The TKE contour in a pipe with the DF. (a) $V_{inlet} = 1.5 \text{ m/s}$; (b) $V_{inlet} = 2.0 \text{ m/s}$; (c) $V_{inlet} = 2.5 \text{ m/s}$.

Figure 11 shows the normalized velocity and TKE under inlet flow conditions. The turbulence intensity generated by the working fluid is similar to the trend in the internal pressure distribution. In areas with high fluid resistance, fluid drag increases and flow separation occur during fluid flow. As a result, it is judged that the flow characteristics deteriorated and the turbulence intensity increased due to the increase in pressure.

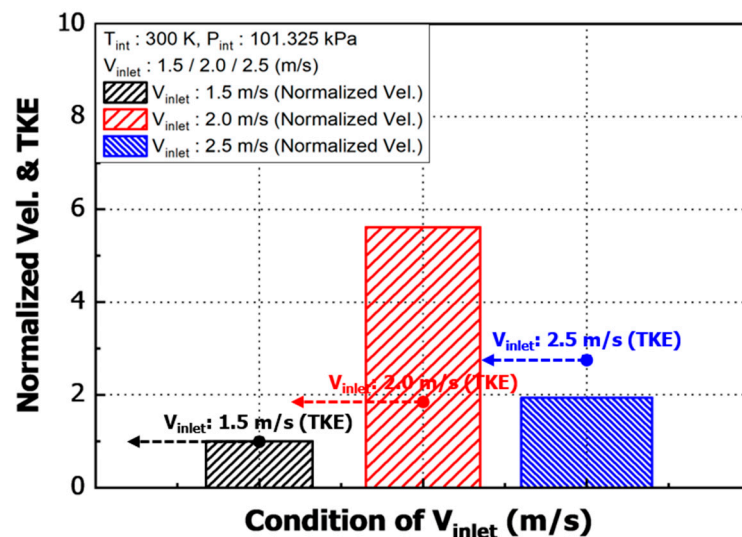


Figure 11. Normalized results for velocity and TKE under various flow velocities.

3.2. Pressure Characteristics of the DF

Figure 12 indicates the pressure distributions for each flow velocity in the pipe with the DF and the pipe without the DF, and Figure 13 presents the pressure variation in the pipe with the DF applied according to the measuring lines. Figure 12 shows that the pressure at the front of the filter tends to increase rapidly as the flow rate increases. This indicates that an increase in the flow velocity leads to an increase in the flow mass rate, and

the pressure rises because the flow mass rate increases in the same volume. Thus, it was confirmed that the differential pressure was also increased by the filter, which could lead to the deterioration of the performance of the condenser.

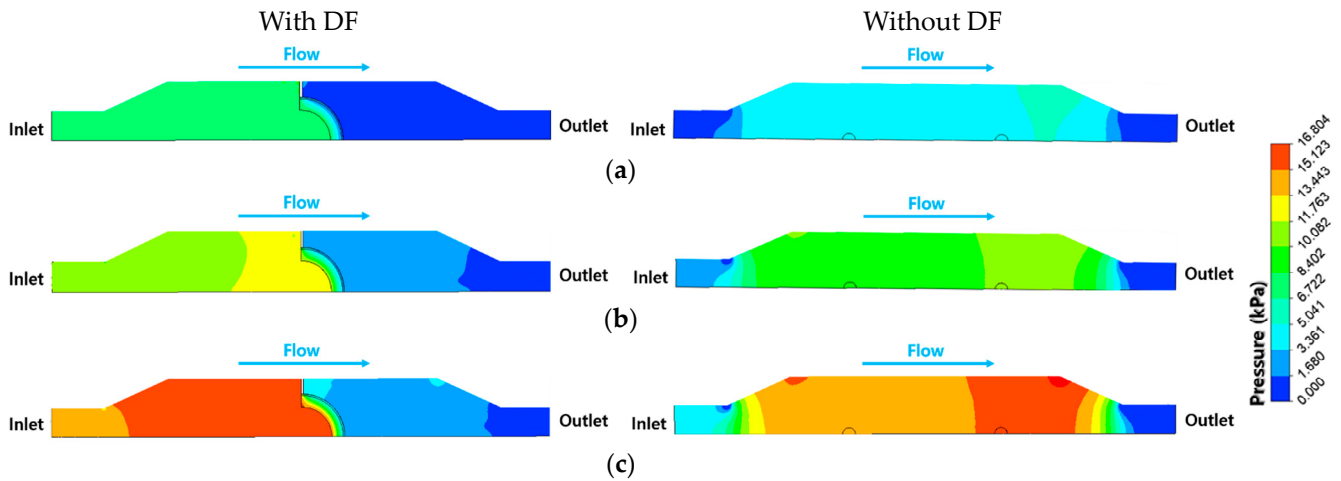


Figure 12. Comparison results of pressure contour with the DF (left) and without the DF (right). (a) $V_{\text{inlet}} = 1.5$ m/s; (b) $V_{\text{inlet}} = 2.0$ m/s; (c) $V_{\text{inlet}} = 2.5$ m/s.

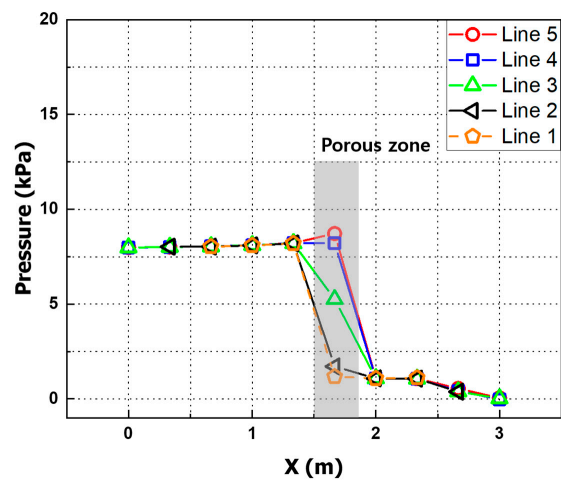
In the pressure distribution in the pipe without the DF in Figure 12, both the inlet and outlet pressures were low, according to Bernoulli's law, and the pressure tended to increase in the part of the expanded pipe where the flow rate was relatively low. On the other hand, in the pipe with the DF, the pressure at the front of the filter increased significantly compared to the case without the DF. It is believed that the pressure inside the pipe is increased significantly by the shape of the filter, the resistance generated by the bracket, and the influence of the pressure drop in the porous zone. It was also determined that the perforated plate of the filter and the shape of the filter have a dominant influence on the differential pressure performance. Thus, further research on this is necessary.

As shown in Figures 9 and 13, as the flow rate increases, the velocity and pressure at the front end of the filter tend to increase. This is because the density per unit area at the outlet point of the pipe increases as the flow rate increases, which increases the kinetic energy of the fluid per the same unit area, meaning that the pressure will be high. At the same initial flow rate condition, the speed and pressure before and after the filter tend to be inversely proportional, and the increase/decrease width for this tends to be large as the flow velocity increases. On the other hand, the velocity and pressure immediately after passing through the porous zone and filter tend to decrease in the same way.

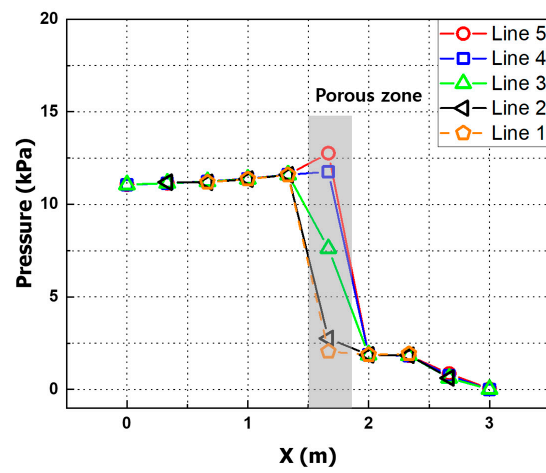
It is understood that the average velocity per area increases as the pressure drop increases, according to Darcy's law, which is generally applied to calculations in porous media. Darcy's law is expressed as Equation (6), where u_D is the average velocity per area of the fluid, Q is the flow rate, A is the cross-sectional area, K is the permeation coefficient, μ is the viscosity coefficient, and P is the pressure [22].

$$u_D = \frac{Q}{A} = -\frac{K \Delta P}{\mu \Delta x} \quad (6)$$

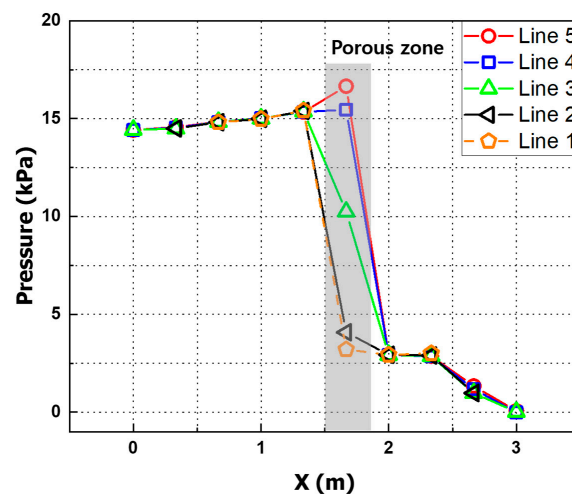
Additionally, in Figure 13, the pressure in the porous zone increases toward the center of the pipe. This is because the flow per unit area near the center increases as the flow in the pipe approaches the maximum flow rate toward the center due to the no-slip condition. The resistance the working fluid receives from the viscous resistance of the filter increases in proportion to the flow rate.



(a)



(b)



(c)

Figure 13. Pressure distributions of pipe with the DF applied. (a) $V_{inlet} = 1.5$ m/s; (b) $V_{inlet} = 2.0$ m/s; (c) $V_{inlet} = 2.5$ m/s.

4. Conclusions

In this study, a numerical analysis method was used to compare and analyze the flow characteristics and differential pressure performance of the CTCS to which a 14-inch DF was applied. As a result, the following conclusions were reached:

(1) The numerical analysis confirmed that the main flow in the pipe with the DF was dominantly affected by the vortex generated by the DF bracket.

(2) As the flow velocity increases, the radius of the vortex generated by the flow colliding with the DF bracket increases. As the vortex radius increases, friction with the main flow is induced, leading to an increase in the TKE, which interferes with the main flow and is thought to cause flow loss in the tube.

(3) According to Bernoulli's law, the pressure before and after the DF tends to be inversely proportional to the flow rate and pressure. On the other hand, the speed and pressure in the filter tend to be proportional, which was confirmed by calculations made using Darcy's law on the influence of the porous zone of the perforated plate.

(4) In addition, it was confirmed that the filter shape and fluid resistance due to a pressure drop in the porous zone had a dominant influence on the differential pressure performance in the pipe with the DF.

Author Contributions: Conceptualization, H.-K.S., D.-W.J. and Y.-C.L.; methodology, D.-W.J., C.-W.S. and Y.-C.L.; software, D.-W.J., C.-W.S. and Y.-C.L.; validation, H.-K.S., D.-S.K. and S.-Y.L.; formal analysis, D.-W.J., C.-W.S. and Y.-C.L.; investigation, H.-K.S., D.-W.J., C.-W.S., Y.-C.L., D.-S.K. and S.-Y.L.; resources, H.-K.S.; data curation, D.-S.K. and S.-Y.L.; writing—original draft preparation, D.-W.J.; writing—review and editing, C.-W.S. and H.-K.S.; visualization, D.-W.J. and Y.-C.L.; supervision, H.-K.S.; project administration, H.-K.S.; funding acquisition, H.-K.S. All authors have read and agreed to the published version of the manuscript.

Funding: This work was supported by the Technology Innovation Program (20018176, Development of heat exchanger cleaning system and automatic operation technology that can reduce energy use of heat exchangers by more than 25%) funded by the Ministry of Trade, Industry and Energy (MOTIE, Korea). This work was also supported by the research grant of the Kongju National University in 2021.

Data Availability Statement: Due to the nature of this research, participants of this study did not agree for their data to be shared publicly and data are only available upon reasonable request.

Conflicts of Interest: The authors declare no conflict of interest.

References

1. Chae, H.M.; Kwon, J.T.; Cha, D.A.; Kwon, O.K. The Measurements of Ball Recovery Rate for the Cleaning Apparatus in Plate Heat Exchanger Using Ceramic Ball. *J. Korean Soc. Power Syst. Eng.* **2014**, *18*, 38–44. [[CrossRef](#)]
2. Nam, K.M.; Kang, S.J. A Comparative Study on Technical Efficiency in the Secondary Energy Industry and a Factor Analysis for Technical Efficiency. *Korean Energy Econ. Rev.* **2015**, *14*, 111–141.
3. Park, S.C.; Lee, I.W. Experimental study on analysis of correlation between void fraction and drag reduction rate in air lubrication ship. *J. Korean Soc. Vis.* **2020**, *18*, 11–17.
4. Alwaeli, M.; Mannheim, V. Investigation into the Current State of Nuclear Energy and Nuclear Waste Management—A State-of-the-Art Review. *Energies* **2022**, *15*, 4275. [[CrossRef](#)]
5. Krūmiņš, J.; Kļaviņš, M. Investigating the Potential of Nuclear Energy in Achieving a Carbon-Free Energy Future. *Energies* **2023**, *16*, 3612. [[CrossRef](#)]
6. Pavlenko, I.; Ciszak, O.; Kondus, V.; Ratushnyi, O.; Ivchenko, O.; Kolisnichenko, E.; Kulikov, O.; Ivanov, V. An Increase in the Energy Efficiency of a New Design of Pumps for Nuclear Power Plants. *Energies* **2023**, *16*, 2929. [[CrossRef](#)]
7. Ibrahim, S.M.A.; Attia, S.I. The influence of condenser cooling seawater fouling on the thermal performance of a nuclear power plant. *Ann. Nucl. Energy* **2015**, *76*, 421–430. [[CrossRef](#)]
8. Alabrudzinski, S.; Markowski, M.; Trafczynski, M.; Urbaniec, K. The influence of fouling build-up in condenser tubes on power generated by a condensing turbine. *Chem. Eng. Trans.* **2016**, *52*, 1225–1230.
9. Pattanayak, L.; Padhi, B.N.; Kodamasingh, B. Thermal performance assessment of steam surface condenser. *Case Stud. Therm. Eng.* **2019**, *14*, 100484. [[CrossRef](#)]
10. Mohammadaliha, N.; Amani, M.; Bahrami, M. Thermal performance of heat and water recovery systems: Role of condensing heat exchanger material. *Clean. Eng. Technol.* **2020**, *1*, 100024. [[CrossRef](#)]

11. Gadhamshetty, V.; Nirmalakhandan, N.; Myint, M.; Ricketts, C. Improving air-cooled condenser performance in combined cycle power plants. *J. Energy Eng.* **2006**, *132*, 81–88. [[CrossRef](#)]
12. Yi, C.S.; Lee, C.W. Development on Cleaning System of Condenser for Nuclear Power Plant by Using Sponge Ball. *J. Korean Soc. Manuf. Process Eng.* **2015**, *14*, 21–26.
13. Jeong, G.C.; Lee, H.S.; Lee, C.W. Numerical analysis of ball strainer screen module blockage effects. *J. Korean Soc. Power Syst. Eng.* **2015**, *19*, 83–89. [[CrossRef](#)]
14. Lee, S.J.; Kim, J.S.; Lee, S.H. A study on the fouling factor and formation of surface film in the power plant condenser. *Korean J. Mater. Res.* **1997**, *7*, 750–757.
15. Kwon, S.Y.; Hur, D.J.; Choi, J.K. A study of the ball dispersion prediction for increasing the effect of condenser tube cleaning system. In Proceedings of the Korean Society for Computational Fluids Engineering Spring Conference, Yeosu, Republic of Korea, 25 May 2016.
16. Kwon, S.Y.; Hur, D.J.; Yun, K.S. Study on the Prediction of Ball Collection Rate in Power Plants Condenser Tube Cleaning System. In Proceedings of the Korean Society of Mechanical Engineers Autumn Conference, Seoul, Republic of Korea, 15 March 2017.
17. Jung, M.S.; Kim, K.T. Debris filtering efficiency and its effect on long term cooling capability. *Nucl. Eng. Des.* **2013**, *261*, 1–9. [[CrossRef](#)]
18. Walker, M.E.; Safari, I.; Theregowda, R.B.; Hsieh, M.K.; Abbasian, J.; Arastoopour, H.; Dzombak, D.A.; Miller, D.C. Economic impact of condenser fouling in existing thermoelectric power plants. *Energy* **2012**, *44*, 429–437. [[CrossRef](#)]
19. Kim, Y.W.; Goo, J.R.; Bae, Y.C.; Lee, H.; Lee, Y.S. Vibration Phenomena between Condensate Vertical Pump and Condenser Debris system in Power Plant. In Proceedings of the Korean Society for Noise and Vibration Engineering Conference, Yongpyong, Republic of Korea, 15 November 2001.
20. Lee, K.Y. Rotor Dynamic Analysis of Brush Seal According to Various Design Parameters Using 3D CFD. Master's Thesis, Gachon University, Seongnam, Republic of Korea, 2019.
21. Contreras, M.L.T.; Lain, S.; Ilinca, A. A review on the estimation of power loss due to icing in wind turbines. *Energies* **2022**, *15*, 1083. [[CrossRef](#)]
22. Choi, S.W.; Yang, J.H.; Kim, B.S.; Kwon, J.S. Study on permeability coefficient and fluid behavior of porous materials. *J. Korean Soc. Mar. Eng.* **2018**, *42*, 742–746. [[CrossRef](#)]

Disclaimer/Publisher's Note: The statements, opinions and data contained in all publications are solely those of the individual author(s) and contributor(s) and not of MDPI and/or the editor(s). MDPI and/or the editor(s) disclaim responsibility for any injury to people or property resulting from any ideas, methods, instructions or products referred to in the content.